ACS Catalysis

Research Article

pubs.acs.org/acscatalysis

Efficient Catalyst for Acceptorless Alcohol Dehydrogenation: Interplay of Theoretical and Experimental Studies

Guixiang Zeng,[†] Shigeyoshi Sakaki,*[,†] Ken-ichi Fujita,*[,‡] Hayato Sano,[‡] and Ryohei Yamaguchi*[,‡]

[†]Fukui Institute for Fundamental Chemistry, Kyoto University, Takano-Nishihiraki-cho 34-4, Sakyo-ku, Kyoto 606-8103, Japan

[‡]Graduate School of Human and Environmental Studies, Kyoto University, Yoshida-Nihonmatsu-cho, Sakyo-ku, Kyoto 606-8501, Japan

Supporting Information

ABSTRACT: The promoterless AAD (acceptorless alcohol dehydrogenation) reaction mediated by an iridium catalyst Cp*Ir(bpyO) **1−Ir** (Cp* = pentamethylcyclopentadienyl, bpyO = α,α'-bipyridonate) has been theoretically investigated with the density functional theory. The reaction occurs through three steps, including alcohol dehydrogenation, formation of dihydrogen complex, and H_2 elimination from the iridium center. In the first two steps, the metal center and the bpyO ligand work cooperatively via the aromatization/dearomatization process of the bpyO ligand. The second step is rate-determining, where the $\Delta G^{0\neq}$ and ΔG^0 values are 23.9 and 13.9 kcal/mol, respectively. Our calculations demonstrate that the aromatization of the bpyO ligand as well as the charge transfer (CT) from the Cp* ligand to the iridium center plays important roles in stabilizing the transition state of the rate-determining step. We have theoretically and experimentally examined the 4d rhodium analogue Cp*Rh(bpyO) **1−Rh** and found that it exhibits similar activity to that of **1−Ir**. On the basis of those results, a new catalyst (HMB)Ru(bpyO) **1−Ru** (HMB = hexamethylbenzene) is designed both theoretically and experimentally, where a cheaper and more abundant 4d ruthenium element is employed with the HMB and bpyO ligands. Theoretical calculations certainly show that **1−Ru** is active for the promoterless AAD reaction via the same reaction mechanism as that of the reaction by **1−Ir**. The experiments also demonstrate that **1−Ru** is as efficient as **1−Ir** for the AAD reaction.

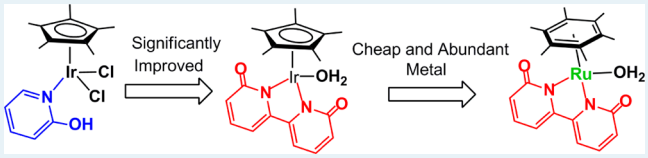

KEYWORDS: *acceptorless alcohol dehydrogenation, theoretical calculation, iridium, cooperative catalysis, rhodium, ruthenium*

INTRODUCTION

The acceptorless alcohol dehydrogenation (AAD) with the release of H_2 provides promising synthetic routes for such carbonyl compounds as aldehydes, ketones, esters, and amides.[1] It also exhibits potential for the H_2 production from biomass and/or its fermentation products, which is crucial for the hydrogen production technology.[2] Various AAD reactions have been reported since its discovery about 40 years ago.[3] In most of them, acid or base promoters are required. For example, a series of the acid-promoted AAD reactions mediated by $Ru(OCOCF_3)_2(CO)(PPh_3)_2$ were reported by Robinson and his co-workers in the 1970s.[3a,b] Subsequently, a variety of base-promoted AAD reactions were reported by Morton and Cole-Hamilton.[3c,d] In these works, the reactions occur on the metal center, while the ligand acts as a spectator.[4]

Owing to the increasing demand for environmentally benign synthetic processes, promoterless AAD reactions are desirable. In recent years, the cooperative catalysts involving combined basic and acidic sites were found to satisfy this requirement. However, examples of the cooperative catalytic cycle have been limited so far. One good example is a series of ruthenium pincer complexes (**Cat1** to **Cat3**) developed by Milstein's group,[5] which catalyze the AAD reactions under neutral reaction conditions; see Scheme 1. A cationic cobalt(II) alkyl complex reported by Hanson's group was also active for the AAD reaction without additives.[6] However, high temperatures (110−120 °C) are needed in these reactions. Since 2007, several iridium complexes (**Cat4** to **Cat6**) have been reported by Yamaguchi, Fujita, and their co-workers, which catalyze the AAD reactions efficiently under mild conditions (reflux in toluene or water), as shown in Scheme 2.[7a−e] In addition, similar catalysts have been reported for transfer hydrogenation, water oxidation, and carbon dioxide hydrogenation.[7f−j] Besides the experimental work, a number of computational works have

Scheme 1. Ruthenium-Based Catalysts for the AAD Reaction Developed by Milstein's Group

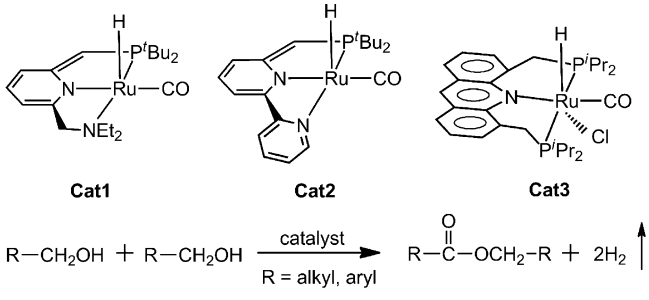

Received: November 24, 2013
Revised: January 30, 2014
Published: February 10, 2014

Scheme 2. Iridium Complexes Employed for the AAD Reaction

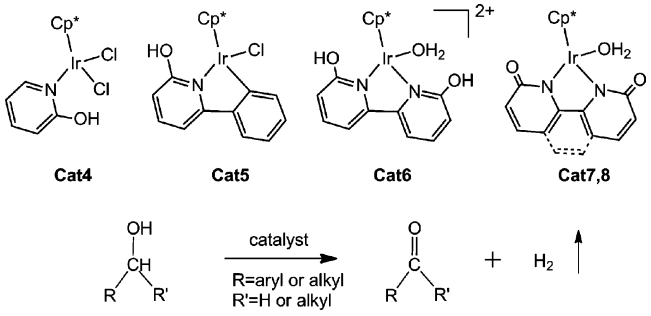

been reported.[8] Those computational studies demonstrate that the promoterless AAD reactions take place under the cooperation of the metal center and the ligand via an aromatization/dearomatization process of the ligand. However, the influence of the aromatization/dearomatization process on the activity of the catalyst has not been discussed.

Recently, Yamaguchi, Fujita, and their co-workers synthesized a more effective iridium complex Cp*Ir(bpyO)(H_2O) **Cat7** (Cp* = pentamethylcyclopentadienyl, bpyO = α,α'-bipyridonate); see Scheme 2.[7d] It works well not only in the AAD reactions of aromatic alcohols but also in the AAD reactions of the aliphatic alcohols under mild conditions. One important difference of **Cat7** from **Cat4** to **Cat6** is the presence of the bipyridonate ligand (bpyO), which is already in an active form unlike the hydroxylpyridine ligand in **Cat4** to **Cat6**; remember that the hydroxylpyridine must undergo deprotonation before the catalytic reaction. On the other hand, the substitution of a phenanthroline-based functional ligand for the bpyO ligand , deprotonated 2,9-dihydroxy-1,10-phenanthroline (phenO), considerably decreases the activity of the catalyst Cp*Ir(phenO)(H_2O) **Cat8**; see Scheme 2 for **Cat8** and the phenO ligand. These results suggest that the activity of this kind of iridium catalyst is sensitive to the ligand and the bpyO ligand is the optimized one so far. However, the reason is not clear. Also, it is unclear whether the mechanism of the AAD reaction by **Cat 7** is the same as that by previously reported catalysts such as **Cat4** or not.

In this work, we theoretically investigated the AAD reactions of primary and secondary alcohols with several iridium complexes to elucidate the reaction mechanism, to explore how much the aromatization/dearomatization process of the ligand influences the activity of the catalyst, and to explain why the activity of the catalyst decreases substantially by the substitution of phenO for bpyO. On the basis of these results, we proposed new AAD catalysts by theoretical work and evaluated their catalytic activities by experiments.

RESULTS AND DISCUSSION

AAD Reaction of Benzyl Alcohol by Cp*Ir(bpyO) 1–Ir.[9] There are two possible reaction pathways for the AAD reaction; one is the outer-sphere pathway and another is the inner-sphere β-H elimination one.[10] Here, we employed the benzyl alcohol **2** as a substrate in calculations.

Outer-Sphere Pathway. In the outer-sphere concerted pathway (see Scheme 3), the AAD reaction occurs by the cooperation of the iridium center and the bpyO ligand, which directly affords a hydride complex Cp*Ir(H)(pyOpyOH) **4–Ir** (pyOpyOH = α-pyridonate-α'-hydroxylpyridine) through a transition state $\mathbf{TS_{1/4}}$**–Ir**, as shown in Figure 1. In $\mathbf{TS_{1/4}}$**–Ir**, the H1 atom migrates from the hydroxyl group (O3–H1) of **2** to the carbonyl O2 atom of the bpyO ligand, where the O3–H1 distance increases to 1.295 Å and the O2–H1 distance decreases to 1.120 Å. At the same time, the H2 atom migrates to the iridium center from **2**, where the Ir–H2 distance shortens to 1.682 Å and the C2–H2 distance lengthens to 1.524 Å. These geometrical features suggest that the O3–H1 and C2–H2 bonds are being broken, but the O2–H1 and Ir–H2 bonds are being formed in $\mathbf{TS_{1/4}}$**–Ir**. On the other hand, the C2═O3 double bond is partially formed (1.278 Å) concomitantly with the weakening of the O3–H1 and C2–H2 bonds. In **4–Ir**, the O2–H1 and Ir–H2 bonds are formed, where the bond distances are 0.992 and 1.595 Å, respectively. In this step, benzaldehyde **3** is released. The $\Delta G^{0\neq}$ and ΔG^0 values of this reaction step are 12.6 and 3.5 kcal/mol, respectively, as shown in Figure 2A.

In this reaction step, the pyridonate moiety of the bpyO ligand is converted to a hydroxylpyridine moiety through the protonation of the carbonyl O2 atom, which corresponds to the aromatization of the pyridonate moiety.[11] Actually, the geometry of the C_5N ring of the hydroxylpyridine moiety is essentially the same as that of the free hydroxylpyridine molecule; see Figure S3 in Supporting Information for the optimized geometry of hydroxylpyridine. The Ir–N1 bond is elongated by 0.050 Å when going from **1–Ir** to **4–Ir**; see Figure 1. The neutral hydroxylpyridine moiety in **4–Ir** is less electron-donating than the anionic pyridonate moiety in **1–Ir**. Also, the Ir–H2 bond formation weakens this N1→Ir charge transfer (CT) interaction, because the hydride H2 ligand is

Scheme 3. Proposed Reaction Pathways of the AAD Reaction Mediated by Cat 7

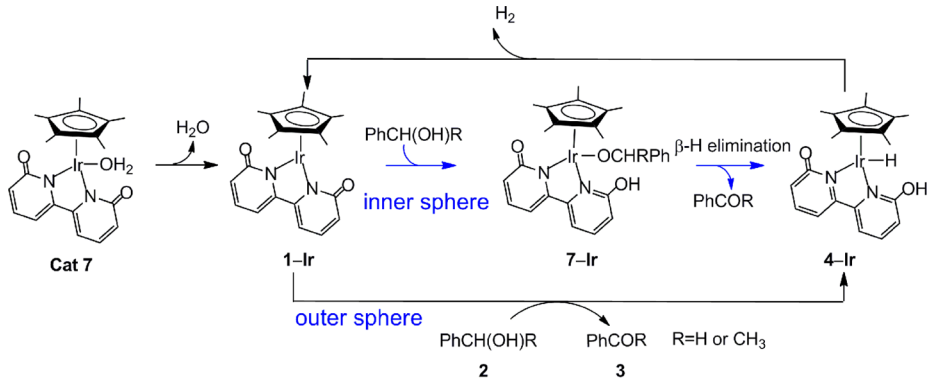

dx.doi.org/10.1021/cs401101m | ACS Catal. 2014, 4, 1010–1020

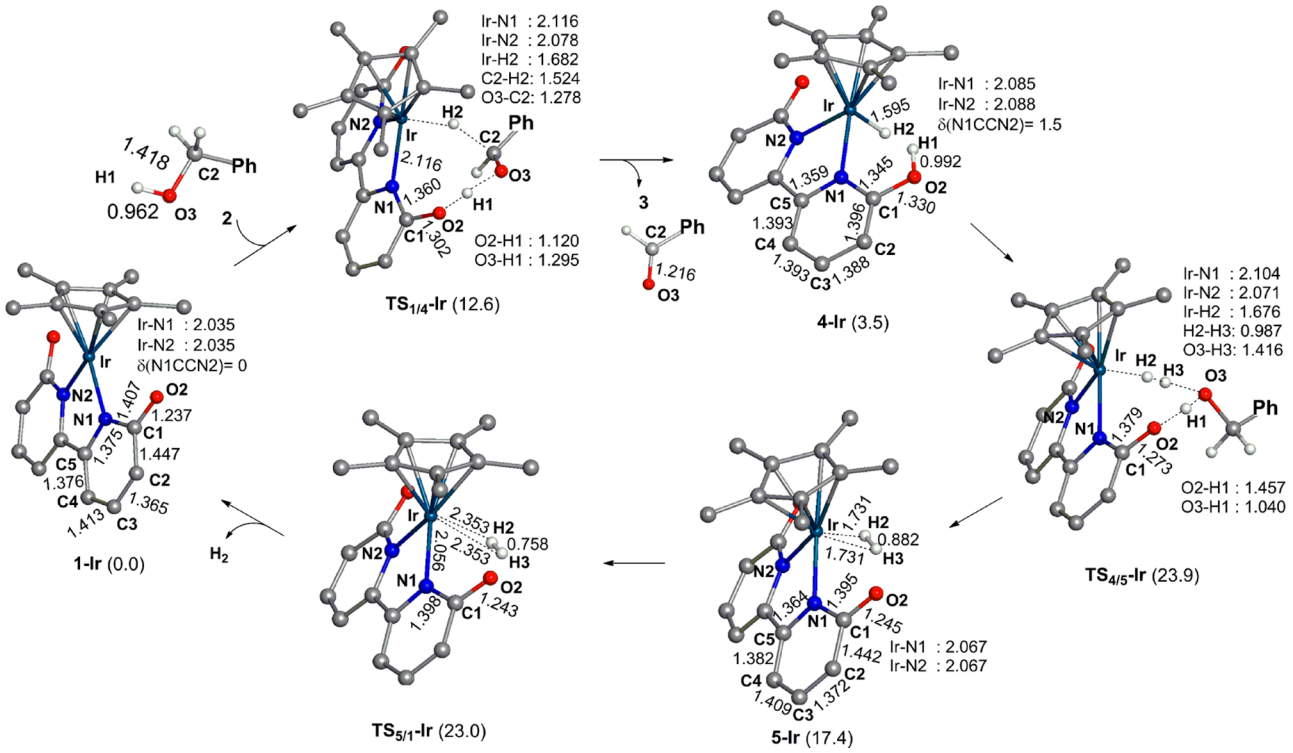

Figure 1. Geometry and energy changes of the AAD reaction of the benzyl alcohol **2** by Cp*Ir(bpyO) **1**−**Ir** along the outer-sphere concerted pathway. Hydrogen atoms on the Cp* and bpyO ligands are omitted for clarity. Bond distances are in angstrom. In parentheses are Gibbs energy changes (in kcal/mol).

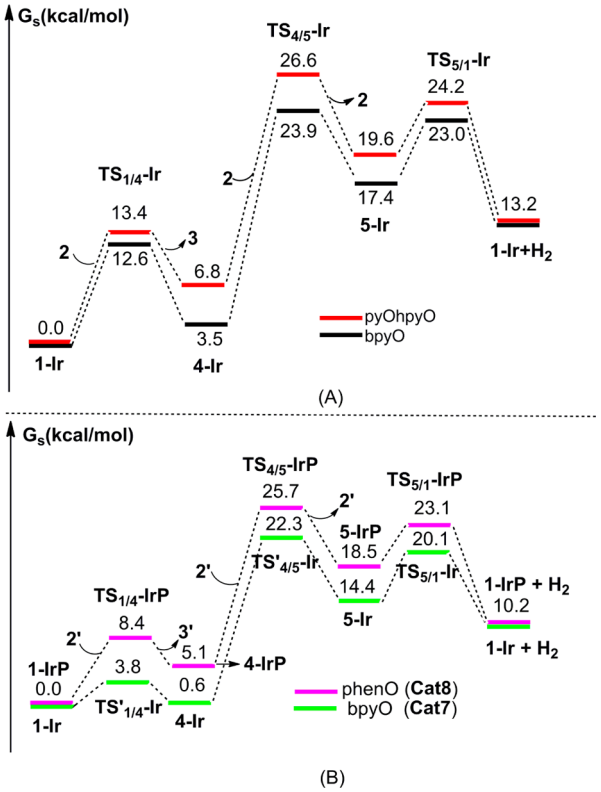

Figure 2. (A) Reaction profile for the AAD reaction of benzyl alcohol **2** mediated by Cp*Ir(bpyO) **1**−**Ir** and Cp*Ir(pyOhpyO) **1**−**IrH**. (B) Reaction profile for the AAD reaction of 1-phenylethanol **2**′ mediated by Cp*Ir(bpyO) **1**−**Ir** (**Cat7**) and Cp*Ir(phenO) **1**−**IrP** (**Cat8**).

strongly electron-donating. Due to these two factors, the Ir−N1 bond is elongated.

The next step is the formation of a dihydrogen complex Cp*Ir(bpyO)(H_2) **5**−**Ir**. This process is facilitated by an alcohol bridge, which occurs through a transition state **TS**$_{4/5}$−**Ir**, as shown in Figure 1. In **TS**$_{4/5}$−**Ir**, the protonic H1 atom migrates from the hydroxyl O2 atom of the ligand to the hydroxyl O3 atom of the bridging alcohol molecule, where the O2−H1 and O3−H1 distances are 1.457 and 1.040 Å, respectively. Simultaneously, the protonic H3 atom migrates from the hydroxyl O3 atom to the hydride H2 ligand, where the O3−H3 and H2−H3 distances are 1.416 and 0.987 Å, respectively. In **TS**$_{4/5}$−**Ir**, the Ir−H2 bond length increases to 1.676 Å, comparing with that (1.595 Å) in **4**−**Ir**. These geometrical features indicate that the H2−H3 bond is being formed concomitantly with the Ir−H2 bond breaking in **TS**$_{4/5}$−**Ir**. In **5**−**Ir**, the Ir−H2 bond is further elongated to 1.731 Å, whereas the H2−H3 bond distance further decreases to 0.882 Å. These geometrical changes indicate that a dihydrogen complex is formed. This reaction step occurs with a $\Delta G^{0\neq}$ value of 23.9 kcal/mol and a ΔG^{0} value of 13.9 kcal/mol.

The deprotonation of the pyOpyOH ligand leads to the dearomatization of the pyOH moiety, as follows: The C1−O2 bond returns back to a double bond (1.245 Å) in **5**−**Ir** from a single bond (1.330 Å) in **4**−**Ir**. The C1−N1 conjugated double bond simultaneously changes to a single bond (1.395 Å). Also, the C1−C2 and C3−C4 bonds become longer, but the C2−C3 and C4−C5 bonds become shorter. These features indicate that the aromatic nature of the C_5N ring disappears in **5**−**Ir**.

We also investigated the transformation of **4**−**Ir** to **5**−**Ir** without the alcohol bridge; see Figure S4 for the geometry of the transition state.[12] In this case, the $\Delta G^{0\neq}$ value increases to

dx.doi.org/10.1021/cs401101m | ACS Catal. 2014, 4, 1010−1020

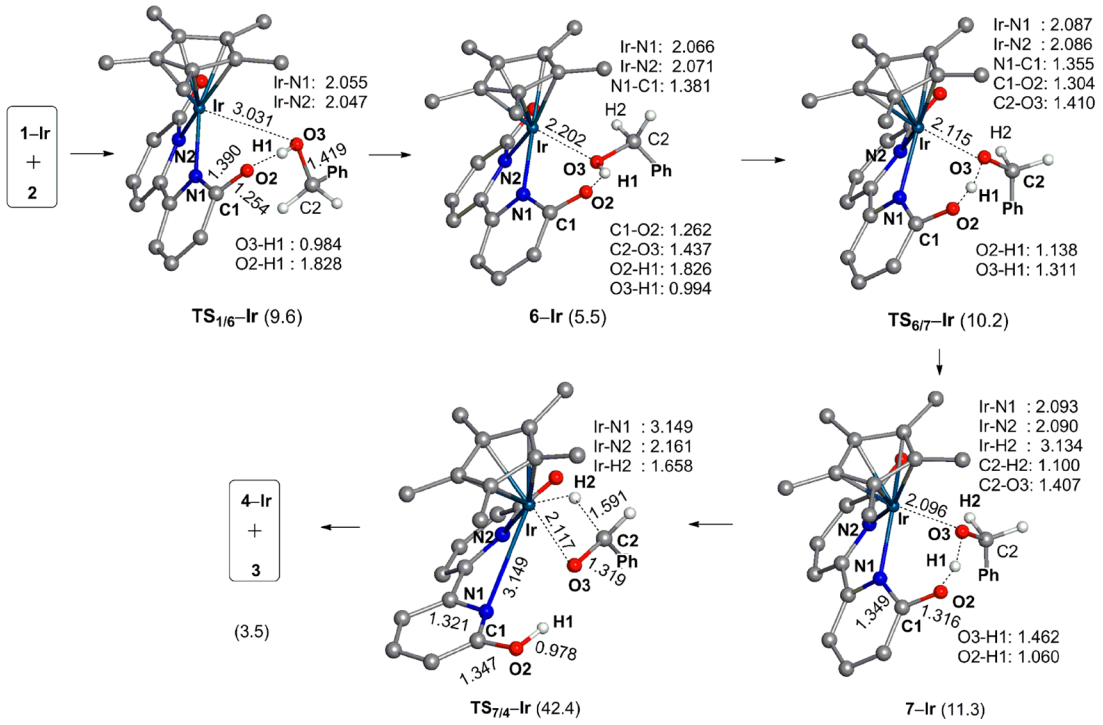

Figure 3. Geometry and energy changes of the AAD reaction of the benzyl alcohol **2** by Cp*Ir(bpyO) **1**–**Ir** along the inner-sphere β-H elimination pathway. Hydrogen atoms on the Cp* and bpyO ligands are omitted for clarity. Bond distances are in angstrom. In parentheses are Gibbs energy changes (in kcal/mol).

31.0 kcal/mol, indicating that the direct formation of the dihydrogen complex is difficult.

The last step is the H_2 elimination from the iridium center through a transition state $\mathbf{TS_{5/1}}$–**Ir** to regenerate the active species **1**–**Ir**. When going from **5**–**Ir** to $\mathbf{TS_{5/1}}$–**Ir**, the Ir–H2 and Ir–H3 distances are significantly elongated to 2.353 and 2.353 Å, respectively, and the H2–H3 distance (0.758 Å) becomes almost the same as that (0.748 Å) of the free H_2 molecule. This reaction step occurs with the $\Delta G^{0\neq}$ and ΔG^0 values of 23.0 and −4.2 kcal/mol, respectively; see Figure 2A.

The outer-sphere stepwise pathway was also investigated here, where the O2–H1 and C2–H2 bonds are cleaved successively in a stepwise manner via an ion pair intermediate; see Scheme S1 in the Supporting Information. However, the ion pair intermediate could not be calculated as an equilibrium species, indicating that this mechanism is not favorable.

Inner-Sphere β-H Elimination Pathway. In the first step of this pathway, the benzyl alcohol **2** coordinates with the iridium center of **1**–**Ir** via the oxygen atom to form a precursor complex Cp*Ir(bpyO)($PhCH_2OH$) **6**–**Ir**; see Scheme 3. When going from $\mathbf{TS_{1/6}}$–**Ir** to **6**–**Ir**, the Ir–O3 distance becomes significantly shorter from 3.031 Å to 2.202 Å, indicating that **2** certainly coordinates with the iridium center; see Figure 3. As a result, the O3–H1 bond is activated, where the bond distance becomes longer by 0.032 Å in **6**–**Ir** than in the free alcohol molecule **2**. The $\Delta G^{0\neq}$ and ΔG^0 values of this coordination step are 9.6 and 5.5 kcal/mol, respectively.

In the next step, the H1 atom moves from the hydroxyl O3 atom of **2** to the carbonyl O2 atom of the bpyO ligand, leading to an alkoxide complex Cp*Ir(pyOpyOH)(OCH_2Ph) **7**–**Ir**. In the transition state $\mathbf{TS_{6/7}}$–**Ir**, the O3–H1 and O2–H1 distances are 1.311 and 1.138 Å, respectively. The natural atomic charges of O2, H1, and O3 atoms are −0.738, 0.538, and −0.728 *e*, respectively, suggesting that this is a proton transfer process. In **7**–**Ir**, the Ir–O3 distance is shorter by 0.106 Å than that in **6**–**Ir**, indicating that the alkoxide moiety more strongly coordinates with the iridium center than the alcohol molecule, as expected. The $\Delta G^{0\neq}$ and ΔG^0 values of this step are 10.2 and 5.8 kcal/mol, respectively.

In the third step, the β-C–H bond of the alkoxide moiety is activated through a transition state $\mathbf{TS_{7/4}}$–**Ir** to produce a hydride complex **4**–**Ir** with the release of benzaldehyde **3**. When going from **7**–**Ir** to $\mathbf{TS_{7/4}}$–**Ir**, the Ir–O3–C2 angle significantly decreases from 125° to 78°, which makes the C2–H2 bond approach the iridium center. Actually, the Ir–H2 distance significantly decreases from 3.134 to 1.658 Å. As the C2–H2 bond approaches the iridium center, its bond distance considerably increases from 1.100 to 1.591 Å. At the same time, the C2–O3 distance somewhat decreases to 1.319 Å from 1.407 Å, indicating that the C2–O3 bond becomes stronger. This β-C–H activation step occurs with the $\Delta G^{0\neq}$ and ΔG^0 values of 42.4 and −7.8 kcal/mol, respectively. The $\Delta G^{0\neq}$ value is too large for this reaction pathway to occur at the experimental temperature (353.15 K). Hence, this mechanism can be excluded.

The above result is different from the previous computational result of the AAD reaction by **Cat4**, in which the inner-sphere β-H elimination pathway occurs with comparable $\Delta G^{0\neq}$ value to that of the outer-sphere concerted pathway.[8b] In the active form of **Cat4**, a monodentate pyridonate ligand coordinates with the iridium center, which changes to a hydroxylpyridine ligand in the proton transfer step. The hydroxylpyridine ligand may easily dissociate from the iridium center to generate enough space for the following β-H elimination reaction. This is favorable for the inner-sphere β-H elimination mechanism. In **Cat7**, however, the bpyO lignad changes to a pyOpyOH ligand in the proton transfer step. The pyOpyOH would not completely dissociate from the iridium center, because the

dx.doi.org/10.1021/cs401101m | ACS Catal. 2014, 4, 1010–1020

pyOpyOH is a chelating ligand and the remaining pyO moiety strongly coordinates with the iridium center (see Figure 3). As a result, the structure around the iridium center is congested in $\mathbf{TS}_{7/4}$**−Ir**. Moreover, the pyOH moiety would partially dissociate from the iridium center to keep the six-coordinate structure of the iridium center in the β-H abstraction step, which further destabilizes $\mathbf{TS}_{7/4}$**−Ir**; remember that the iridium center takes a d^6 electron configuration. Because of these two factors, the β-H elimination pathway needs a considerably large $\Delta G^{0\neq}$ value in the **Cat7**-catalyzed AAD reaction. However, the catalytic efficiency of **Cat4** is lower than **Cat7**. This is because **Cat4** must undergo the successive HCl elimination and the ligand rotation to generate the active form of the catalyst. These processes increase the energy barrier of the AAD reaction by **Cat4**,[8b] which leads to the lower catalytic efficiency of **Cat4** than that of **Cat7**.

As discussed above, the outer-sphere concerted pathway is more favorable than the inner-sphere β-H elimination one in the AAD reaction by **Cat7**. In the former case, the formation step of dihydrogen complex (**4−Ir** to **5−Ir**) is the rate-determining step with a $\Delta G^{0\neq}$ value of 23.9 kcal/mol.[13] In the latter case, the rate-determining step is the β-C−H bond activation step (**7−Ir** to **4−Ir**) with a $\Delta G^{0\neq}$ value of 42.4 kcal/mol.

Electron Redistribution along the Outer-sphere Concerted Pathway. In the dehydrogenation step, the H2 atom migrates from the alcohol to the iridium center to form an Ir−H2 bond, and the H1 atom moves to the carbonyl oxygen (O2) atom of the bpyO ligand to form an O2−H1 bond, as discussed above. These geometrical changes occur with considerably large population changes. The iridium atomic population considerably increases when going from **1−Ir** to **4−Ir**, as shown in Figure 4. This is because the CT occurs from the H2 ligand to the iridium center. Such CT suppresses the CT from the Cp* ligand to the iridium center, which leads to an increase in the electron population of the Cp* ligand. On the other hand, the electron population of the active C_5N(a) ring considerably decreases, whereas that of the inactive C_5N(b) ring decreases little. This is because the protonation of the carbonyl O2 atom induces the aromatization of the anionic pyridonate moiety to a neutral hydroxylpyridine moiety. Unexpectedly, the O2 atomic population changes little, even though the protonation occurs at the O2 atom. This phenomenon indicates that the protonic H1 atom is mainly provided electron population by the C_5N(a) ring, which is consistent with the decrease in the electron population of the C_5N(a) ring.

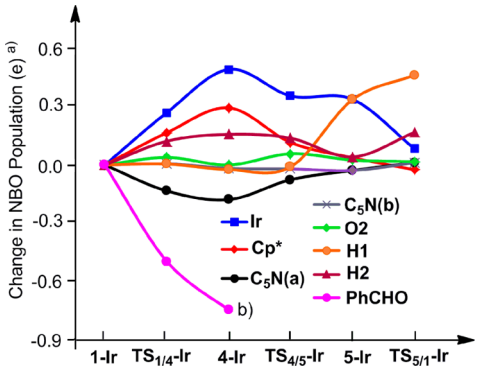

Figure 4. NBO population changes of Ir, Cp*, C_5N(a), C_5N (b), and O2 along the outer-sphere concerted pathway of the AAD reaction of benzyl alcohol **2** by Cp*Ir(bpyO) **1−Ir**. C_5N(a) and C_5N(b) represent the active C_5N and inactive C_5N rings, respectively. (a) A positive value represents an increase in electron population relative to **1−Ir**, and vice versa. (b) The electron population of aldehyde PhCHO does not change after here, because it releases from the reaction system in the dehydrogenation step of alcohol.

In the formation step of the dihydrogen complex, the strongly electron-donating hydride ligand changes to a weakly electron-donating dihydrogen ligand. As a result, the iridium atomic population somewhat decreases, when going from **4−Ir** to **5−Ir**, as shown in Figure 4. To compensate for the decrease in the iridium atomic population, the CT starts to occur from the Cp* ligand to the iridium center. This is the origin of the decrease in the electron population of the Cp* ligand. Simultaneously, the electron population of the active C_5N(a) ring somewhat increases, which corresponds to the dearomatization of the neutral hydroxylpyridine moiety to the anionic pyridonate moiety. These population changes indicate that the CT from the Cp* ligand to the iridium center contributes to the stabilization of $\mathbf{TS}_{4/5}$**−Ir** in the formation step of the dihydrogen complex, which is rate-determining in the AAD reaction.

In the H_2 elimination step, the dihydrogen molecule dissociates from the iridium center to regenerate the active species **1−Ir**. In this step, the electron population of the iridium center further decreases, because the CT from the dihydrogen molecule to the iridium center gradually disappears. As a result, the CT from the Cp* ligand to the iridium center becomes stronger, which leads to a further decrease in the electron population of the Cp* ligand, as shown in Figure 4.

According to the above analysis, the Cp* ligand receives electrons in the dehydrogenation process and releases them in the rate-determining step to stabilize the corresponding transition state. Hence, the electron-donating Cp* ligand is favorable for the AAD reaction. This is consistent with our calculation results that when the Cp* ligand is substituted for a weaker electron-donating Cp ligand, the Gibbs energy difference between **4−CpIr** and $\mathbf{TS}_{4/5}$**−CpIr** (the rate-determining step) increases to 24.3 kcal/mol; see Figure S5 for the optimized geometries and energy changes.

Effect of Ligand Aromatization/Dearomatization on the Activity of Cp*Ir(bpyO) 1−Ir. To examine how much the aromatization/dearomatization process of the ligand influences the activity of **1−Ir**, we employed a model complex Cp*Ir(pyOhpyO) in the AAD reaction, where the pyOhpyO ligand consists of a pyridonate ring (pyO) and a hydrogenated pyridonate (hpyO) ring, as shown in Figure 5. Cp*Ir(pyOhpyO) is named as **1−IrH**, hereafter. In the following discussion, we investigated the AAD reaction which occurs under the cooperation of the iridium center and the hpyO moiety of the ligand; note that the aromatization/dearomatization process does not occur in the hpyO moiety, because the C_5N ring of the hpyO moiety is saturated with hydrogen atoms.

In **1−IrH**, the Ir−N1 distance is somewhat shorter than that in **1−Ir** by 0.028 Å (as shown in Figure 5), whereas the Ir−N2 bond distance becomes moderately longer by 0.009 Å. These results indicate that the interaction of the iridium center with the nonconjugated hpyO moiety is stronger than that with the conjugated pyO moiety. These are consistent with the fact that the electron population of the hpyO moiety decreases by 0.60 *e* and that of the pyO by 0.52 *e* when the pyOhpyO ligand coordinates with the iridium center; see Table S1 in Supporting

dx.doi.org/10.1021/cs401101m | ACS Catal. 2014, 4, 1010−1020

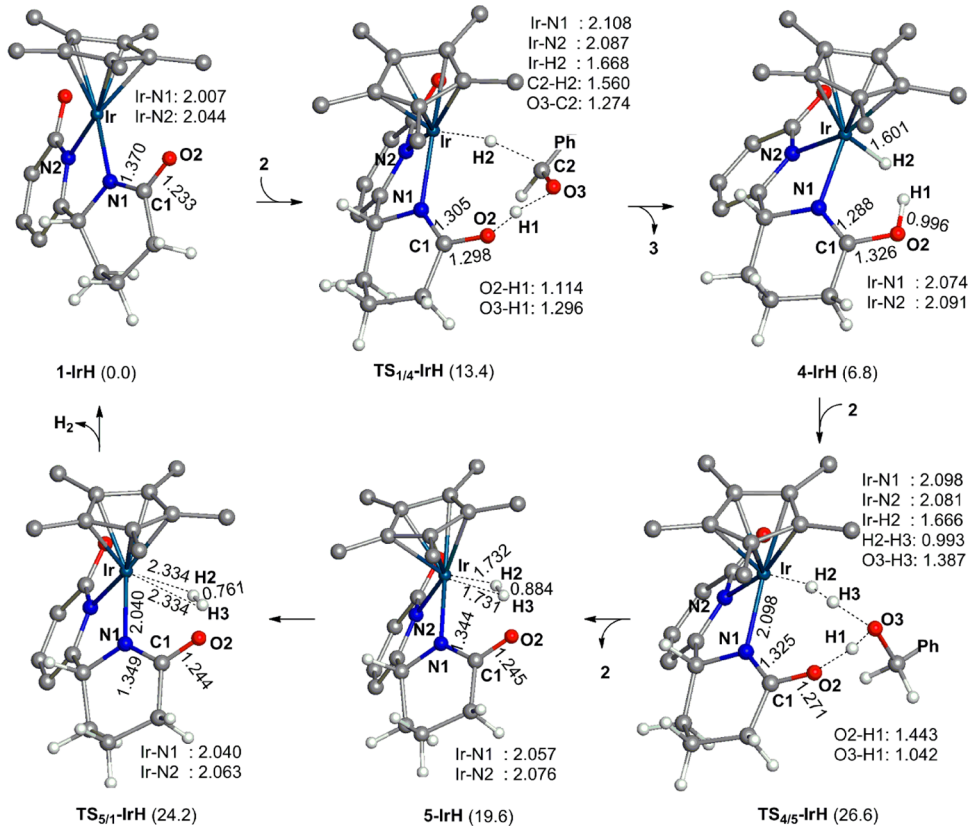

Figure 5. Geometry and energy changes of all the species involved in the AAD reaction of benzyl alcohol **2** mediated by Cp*Ir(pyOhpyO) **1**−**IrH**. Hydrogen atoms on the Cp* ligand and the pyO moiety are omitted for clarity. Bond distances are in angstrom. In parentheses are Gibbs energy changes (in kcal/mol).

Information. This is because the nitrogen lone pair orbital energy is higher in the hpyO moiety than in the pyO moiety; 1.43 eV in the hpyO and 1.22 eV in the pyO, where the Kohn−Sham orbital energies are presented.

The AAD reaction mediated by **1**−**IrH** occurs through a transition state $\mathbf{TS_{1/4}}$−**IrH** to afford a hydride complex **4**−**IrH** with similar geometrical changes to those by **1**−**Ir**, as shown in Figure 5. In this step, the H2 atom migrates from the C2 atom of benzyl alcohol **2** to the iridium center. At the same time, the H1 atom moves from the hydroxyl group of the benzyl alcohol to the carbonyl O2 atom of the hpyO moiety, leading to the formation of a pyOhpyOH ligand. In $\mathbf{TS_{1/4}}$−**IrH**, the C2−H2 and O3−H1 bond distances are elongated to 1.560 and 1.296 Å, respectively, whereas the Ir−H2 and O2−H1 bond distances become shorter to 1.668 and 1.114 Å, respectively. These geometrical features are similar to those in $\mathbf{TS_{1/4}}$−**Ir**; compare Figures 1 and 5. $\mathbf{TS_{1/4}}$−**IrH** is moderately more unstable than $\mathbf{TS_{1/4}}$−**Ir** by 0.8 kcal/mol, whereas the hydride intermediate **4**−**IrH** lies much higher than **4**−**Ir** by 3.3 kcal/mol, as shown in Figure 2(A). These differences indicate that the aromatization of the ligand plays an important role in stabilizing the hydride intermediate.

To understand well how much the aromatization of the ligand influences the relative stabilities of **4**−**Ir** and **4**−**IrH**, we compared the geometries and important bond energies between these two species. In **4**−**IrH**, both the Ir−H2 and O2−H1 bond distances and their bond energies are similar to those in **4**−**Ir**, indicating that the ligand aromatization hardly influences these two bonds; see Scheme S2 and Table S2 in Supporting Information for bond energies. However, a significant difference is found between the hpyOH moiety of the pyOhpyOH ligand in **4**−**IrH** and the corresponding pyOH moiety of the pyOpyOH ligand in **4**−**Ir**, as follows: The C1−N1 bond of the pyOhpyOH ligand becomes shorter by 0.082 Å in the alcohol dehydrogenation step, while that of the bpyO ligand becomes less shorter by 0.062 Å. This is because the π-electron is localized on the C1−N1 bond in the hpyOH moiety for the lack of conjugation; note that the π-electrons are delocalized in the conjugated pyOH ring. These results indicate that the ligand aromatization stabilizes the hydride intermediate through the delocalization of π-electrons.

The next step is the formation of a dihydrogen complex **5**−**IrH** through a transition state $\mathbf{TS_{4/5}}$−**IrH**. In this step, the protonic H1 atom moves from the pyOhpyOH ligand to the O3 atom of the bridging alcohol, and the protonic H3 atom of the bridging alcohol moves toward the H2 hydride ligand to form a H2−H3 bond. $\mathbf{TS_{4/5}}$−**IrH** resembles well $\mathbf{TS_{4/5}}$−**Ir** in geometry. When the most stable species (**1**−**IrH** + **2**) is taken as a reference, the $\Delta G^{0\neq}$ value (26.6 kcal/mol) of $\mathbf{TS_{4/5}}$−**IrH** is higher than that (23.9 kcal/mol) of $\mathbf{TS_{4/5}}$−**Ir**, as shown in Figure 2A. However, the energy difference (19.8 kcal/mol) between **4**−**IrH** and $\mathbf{TS_{4/5}}$−**IrH** is smaller than that (20.4 kcal/mol) between **4**−**Ir** and $\mathbf{TS_{4/5}}$−**Ir**. This is because the dearomatization of the ligand occurs when going from **4**−**Ir** to $\mathbf{TS_{4/5}}$−**Ir** but it does not occur when going from **4**−**IrH** to $\mathbf{TS_{4/5}}$−**IrH**. These results indicate that the less stability of $\mathbf{TS_{4/5}}$−**IrH** than $\mathbf{TS_{4/5}}$−**Ir** arises from the less stability of **4**−**IrH** than **4**−**Ir** (by 3.3 kcal/mol). In brief, the aromatization of the ligand directly stabilizes the hydride intermediate **4**−**Ir**, which in turn leads to the stabilization of the transition state in

dx.doi.org/10.1021/cs401101m | ACS Catal. 2014, 4, 1010−1020

the subsequent formation of a dihydrogen complex (rate-determining step). Thus, the aromatization of the ligand is favorable for the AAD reaction.

The last step is the H_2 elimination from the iridium center to afford the active species **1−IrH**. This process occurs in a similar way in both the bpyO and pyOhpyO systems. We wish to skip the discussion about this step.

Comparison between Activities of Cp*Ir(bpyO) 1−Ir and Cp*Ir(phenO) 1−IrP. The Fujita−Yamaguchi group reported that the catalytic activity of the iridium complex becomes much lower by the substitution of a phenO ligand for the bpyO ligand .[7d] To elucidate the reason, we investigated the AAD reaction of 1-phenylethanol **2′** mediated by Cp*Ir-(phenO) **1−IrP**, which corresponds to **Cat8** reported in the experimental work.[7d] Our calculations indicate that this reaction occurs through the same reaction mechanism as that of the AAD reaction mediated by **1−Ir** via similar geometrical changes. Hence, we skipped the discussion of geometrical changes along the reaction pathway for brevity; see Figure S6 in Supporting Information for optimized geometries.

As shown in Figure 2B, the rate-determining step of the AAD reaction by **1−IrP** is the formation of the dihydrogen complex, as well. Its transition state **TS$_{4/5}$−IrP** lies above **TS′$_{4/5}$−Ir** by 3.4 kcal/mol. This is consistent with the experimental fact that the use of the phenO ligand decreases the activity of the iridium catalyst. It should be noted that the Gibbs energy difference between **4−IrP** and **TS$_{4/5}$−IrP** is smaller than that between **4−Ir** and **TS′$_{4/5}$−Ir**, where **4−IrP** lies above **4−Ir** by 4.5 kcal/mol; see Figure 2B. These results indicate that the dehydrogenation process becomes difficult when the Cp*Ir(phenO) **1−IrP** is employed as a catalyst, because the intermediate **4−IrP** is less stable than **4−Ir**. This is similar to the reaction mediated by Cp*Ir(pyOhpyO) **1−IrH**; compare the energy changes in Figures 2A,B.

It is necessary to explore the reasons why **4−IrP** is less stable than **4−Ir**. One reason is the aromatization effect, which is smaller in the phenO ligand than in the bpyO ligand, because the phenO ligand is more conjugated than bpyO due to the presence of a conjugated six-membered ring between two pyridonate (C_5N) rings. Another reason is that the proton affinity (260.3 kcal/mol) of the phenO ligand is smaller than that (263.7 kcal/mol) of the bpyO ligand by about 3.4 kcal/mol, which is similar to the energy difference between **4−Ir** and **4−IrP**. The smaller proton affinity of the phenO ligand in **1−IrP** comes from the lower orbital energy of the oxygen lone pair (−6.91 eV) than that of the bpyO ligand (−6.77 eV) in **1−Ir**; see Scheme S3 in Supporting Information. It is likely that the phenO ligand stabilizes the oxygen lone-pair orbital more than the bpyO ligand for its larger conjugate electronic structure. As a result, the phenO ligand is less reactive for the protonation reaction than the bpyO ligand, which leads to the less stable intermediate **4−IrP**. In both reasons, the presence of one more six-membered ring in the phenO ligand is the key factor for the lower activity of **1−IrP**.

Prediction of New Catalysts. The prediction of new catalysts was attempted here on the basis of the combination of experimental and theoretical works. The theoretical result will be discussed here first, and the experimental results will be presented below.

The simple and direct way to design a new catalyst with the same ligands as those in Cp*Ir(bpyO) **1−Ir** is to replace the iridium center with its 4d analogue, which is the rhodium element. We examined the reactivity of the complex Cp*Rh-(bpyO) **1−Rh** in the AAD reaction of 1-phenylethanol **2′**; here the secondary alcohol was employed as a substrate, because we were afraid that **1−Rh** was less active than **1−Ir**. The AAD reaction by **1−Rh** occurs with similar geometry and energy changes to those of the reaction by **1−Ir**; see Figure S7 in Supporting Information. The rate-determining step is the formation of the dihydrogen complex like that in the catalytic cycle by **1−Ir**, where the $\Delta G^{0\neq}$ and ΔG^0 values are 21.2 and 12.4 kcal/mol, respectively, relative to the sum of **1−Rh** and **2′**. These $\Delta G^{0\neq}$ and ΔG^0 values are similar to those of the AAD reaction of **2′** mediated by **1−Ir** (22.3 and 13.8 kcal/mol, respectively); see Figure S8. These calculation results indicate that **1−Rh** would be a good candidate for the AAD reaction, which is consistent with the experimental results reported below.

Encouraged by the good result about the rhodium catalyst, we tried to use other 4d metal elements such as ruthenium in the catalyst. The ruthenium element is less expensive and more abundant than the iridium element, which is widely employed in the hydrogen transfer catalyst.[7f,h,14] However, the simple substitution of the iridium(III) center for a ruthenium(II) leads to the formation of a negatively charged ruthenium(II) complex, as shown in Scheme 4. Because the solubility to

Scheme 4. Prediction of a New Catalyst

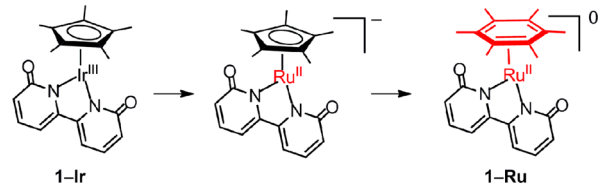

organic solvent is important, a neutral ruthenium(II) complex would be better. This requires to substitute some neutral three-coordinate ligand for the monoanionic Cp* ligand; remember that the ruthenium(II) center is in d^6 electron configuration, which tends to take a six-coordinate octahedral-like structure. One of the candidates is benzene, which is employed in the ruthenium catalyst for transfer hydrogenation reaction.[15] According to the above discussion, the electron-donating ligand is more favorable for the AAD reaction. Therefore, we use hexamethylbenzene (HMB) instead of benzene as a ligand to construct a ruthenium complex; see Scheme 4. The activity of the new ruthenium(II) complex (HMB)Ru(bpyO) **1−Ru** is examined by the AAD reaction of the 1-phenylethanol **2′**.

In the first step, the AAD reaction occurs with the cooperation of the ruthenium center and the bpyO ligand to afford a hydride intermediate (HMB)RuH(pyOpyOH) **4−Ru** through a transition state **TS$_{1/4}$−Ru**; see Figure 6. In **TS$_{1/4}$−Ru**, the H2 atom is moving from the C2 atom to the ruthenium center. Simultaneously, the protonic H1 atom is moving from the O3 atom of the 1-phenylethanol to the carbonyl O2 atom of the bpyO ligand. The geometrical changes of this dehydrogenation step are similar to those of the reaction by **1−Ir**. However, this step much more easily occurs by **1−Ru** with a $\Delta G^{0\neq}$ value of 1.6 kcal/mol than that by **1−Ir** ($\Delta G^{0\neq}$ = 12.6 kcal/mol). In the following, **4−Ru** is converted to a dihydrogen complex (HMB)Ru(bpyO)(H_2) **5−Ru** through an alcohol-bridged transition state **TS$_{4/5}$−Ru**, which is similar to **TS′$_{4/5}$−Ir**. This step occurs with the $\Delta G^{0\neq}$ and ΔG^0 values of 16.7 and 7.9 kcal/mol, respectively, where the sum of **4−Ru** and **2′** is taken as a reference (energy zero); see Figure 6. This

dx.doi.org/10.1021/cs401101m | ACS Catal. 2014, 4, 1010−1020

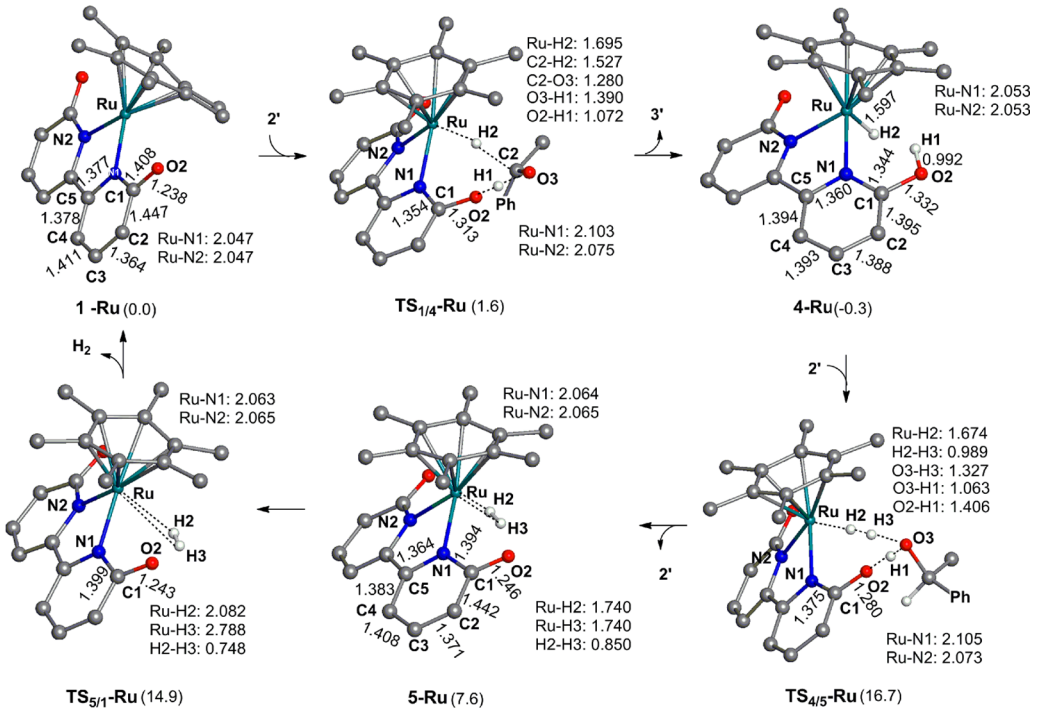

Figure 6. Geometry and energy changes of all the species involved in the AAD reaction of 1-phenylethanol **2′** mediated by (HMB)Ru(bpyO) **1−Ru**. Hydrogen atoms on the HMB and bpyO ligands are omitted for clarity. Bond distances are in angstrom. In parentheses are Gibbs energy changes (in kcal/mol).

$\Delta G^{0\neq}$ value is moderately smaller than that (22.3 kcal/mol) for **TS′$_{4/5}$−Ir**. The last step is the H_2 elimination from the ruthenium center in **5−Ru**, which occurs through a transition state **TS$_{5/1}$−Ru** to regenerate the active species **1−Ru**. This step needs a moderately smaller $\Delta G^{0\neq}$ value (15.2 kcal/mol) than that of the rate-determining step like those in the reactions by **1−Ir** and **1−Rh**. The population changes are also similar to those of the iridium reaction system; see Figure S9 in Supporting Information. These results suggest that the AAD reaction by **1−Ru** occurs with similar electronic processes to those by **1−Ir**.

On the basis of the geometrical and energy changes along the AAD reaction, we reached the conclusion that **1−Ru** would be a good catalyst for the AAD reaction. The experimental results of **1−Ru** will be presented below.

Experiments of AAD Reaction with Cp*Rh(bpyO)(H$_2$O) Cat9 and (HMB)Ru(bpyO)(H$_2$O) Cat10. In order to carry out the experimental study on the theoretically predicted catalyst, we first attempted the synthesis of new catalysts Cp*Rh(bpyO)(H_2O) **Cat9** and (HMB)Ru(bpyO)(H_2O) **Cat10**. The rhodium **Cat9** was synthesized in good yield starting with [Cp*Rh(H_2O)$_3$](OTf)$_2$ by a procedure similar to that for the iridium **Cat7**; see the experimental section. The ruthenium **Cat10** could also be synthesized in a reasonable yield starting with [(HMB)Ru(H_2O)$_3$](OTf)$_2$ via [(HMB)Ru(6,6′-dihydroxy-2,2′-bipyridine)(H_2O)](OTf)$_2$. Then, we performed experiments of the AAD reaction catalyzed by **Cat9** and **Cat10**, using 1-phenylethanol as a substrate. For comparison, a similar reaction catalyzed by the previous iridium catalyst, Cp*Ir(bpyO)(H_2O) **Cat7**, was also carried out. Results are summarized in Table 1. When the solution of 1-phenylethanol in benzene (boiling point: 80 °C) was refluxed for 20 h in the presence of 0.50 mol % of **Cat7**, acetophenone was obtained quantitatively along with the evolution of hydrogen gas (entry 1).[16,17a] Analogous rhodium **Cat9** also showed high catalytic activity to give acetophenone in 95% yield (entry 2), supporting the theoretical prediction described above. The AAD reaction catalyzed by ruthenium **Cat10** resulted in 97% yield of acetophenone (entry 3), also in accord with the theoretical prediction.[17b]

Table 1. Catalytic Performances of Cat7, Cat9, and Cat10 in the AAD Reaction of 1-Phenylethanol under Reflux in Benzene[a]

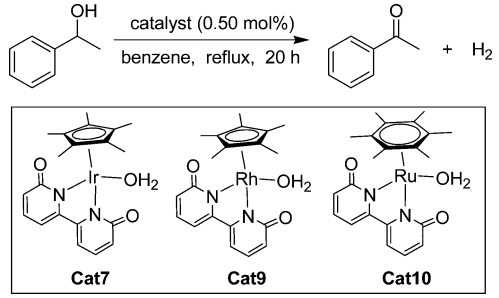

entry	catalyst	conversion (%)[b]	yield (%)[b]
1	**Cat7**	100	100
2	**Cat9**	95	95
3	**Cat10**	97	97

[a]The reaction was carried out with catalyst (0.50 mol %) and 1-phenylethanol (1.0 mmol) in benzene (3 mL) under reflux for 20 h. [b]Determined by GC.

CONCLUSIONS

In this work, we theoretically investigated the promoterless AAD reactions mediated by Cp*Ir(bpyO) **1−Ir** developed by Yamaguchi, Fujita, and their co-workers, and we theoretically

dx.doi.org/10.1021/cs401101m | ACS Catal. 2014, 4, 1010−1020

and experimentally found new catalysts with the rhodium and ruthenium elements.

The AAD reaction of benzyl alcohol **2** by **1−Ir** occurs through three steps: alcohol dehydrogenation, formation of dihydrogen complex, and elimination of dihydrogen molecule. In the first step, the outer-sphere concerted pathway is more favorable than the inner-sphere β-H elimination pathway, which is different from the reaction mechanism of the AAD reaction by a Cp*Ir(pyridonate) complex **Cat4** (see Scheme 2). The second step is facilitated by an alcohol bridge. In these two steps, the metal center and the bpyO ligand work cooperatively via the aromatization and dearomatization processes of the ligand. The second step is rate-determining, where the $\Delta G^{0\neq}$ and ΔG^{0} values are 23.9 and 13.9 kcal/mol, respectively.

When the pyOhpyO ligand is employed in the catalyst instead of the bpyO ligand, the $\Delta G^{0\neq}$ value of the rate-determining step becomes higher to 26.6 kcal/mol. This is because one hpyO ring of the pyOhpyO ligand is saturated with hydrogen atoms and the aromatization/dearomatization of the ligand does not occur in the AAD reaction. When the bpyO ligand is substituted for a larger conjugated phenO ligand, the rate-determining step also becomes more difficult; the $\Delta G^{0\neq}$ value is 25.7 kcal/mol. This result arises from the smaller proton affinity of the oxygen atom and smaller aromatization effect of the phenO ligand.

We proposed new AAD catalysts, Cp*Rh(bpyO) **1−Rh** and (HMB)Ru(bpyO) **1−Ru**, with the combination of the theoretical results and experimental intuition. Both theoretical calculations and experimental results show that these complexes are good catalysts for the AAD reaction. The AAD reaction by **1−Rh** occurs with similar geometry and energy changes to those by **1−Ir**, where the $\Delta G^{0\neq}$ value of the rate-determining step is 21.2 kcal/mol. The AAD reaction by **1−Ru** occurs with similar $\Delta G^{0\neq}$ value of 17.0 kcal/mol for the rate-determining step. These results strongly suggest that the main structure of M(bpyO) is crucial and can be applied to a new catalyst for the AAD reactions.

COMPUTATIONAL DETAILS

Geometry optimizations were performed by the density functional theory (DFT)[18] with the B3PW91 functional[19] in the gas phase. The effective core potentials (ECPs) of the Stuttgart−Dresden−Bonn group[20] were employed for the core electrons of the iridium, rhodium, and ruthenium elements. The (311111/22111/411/11) basis sets were used for their valence electrons.[21] The 6-31+G* basis sets[22] were employed for the Cp* group and the phenyl group of benzyl alcohol and 1-phenylethanol. For other atoms, 6-31++G** basis sets[22] were used. Frequency calculation was carried out for each stationary structure to make sure whether it is an equilibrium structure or a transition state. The solvent effect of benzene was evaluated with the conductor-like polarizable continuum model (CPCM),[23] where optimized structures in gas phase were employed. The Gibbs energy in solution was employed for discussion, where the translational entropy was evaluated with the method developed by Whitesides et al.,[24] similar to our previous works.[25] The natural bond orbital analysis was performed for the electron population. All these calculations were carried out by the Gaussian 09 program.[26]

The reliability of the method employed in this work was evaluated by the calculations of the AAD reaction of ethanol by Cp*Ir(bpyO) **1−Ir**. The geometries were optimized by the B3PW91 functional in the gas phase; see Figure S1 in Supporting Information. The energy barrier of the rate-determining step was evaluated by the SCS-MP2,[27] MP2[28] to MP4SDQ[29] methods in solution phase with the CPCM model. As shown in Table S3 in Supporting Information, the B3PW91-calculated results are close to the MP4SDQ-calculated ones. Hence, the B3PW91 functional was employed in all the calculations in this work.

EXPERIMENTAL DETAILS

^{1}H and ^{13}C NMR spectra were recorded on JEOL ECX-500 and ECS-400 spectrometers. Gas chromatography (GC) analyses were performed on a GL-Sciences GC353B gas chromatograph with a capillary column (GL-Sciences InertCap Pure WAX). Elemental analyses were carried out at the Microanalysis Center of Kyoto University. $[Cp^*Rh(H_2O)_3](OTf)_2$,[30] 6,6′-dihydroxy-2,2′-bipyridine,[31] and **Cat7**[7d] were prepared according to the literature method. Organic solvents were dried by standard procedures prior to use. All other reagents are commercially available and were used as received.

Preparation of [Cp*Rh(6,6′-dihydroxy-2,2′-bipyridine)(H$_2$O)](OTf)$_2$. Under an atmosphere of argon, $[Cp^*Rh(H_2O)_3](OTf)_2$ (0.384 g, 0.65 mmol) was placed in a flask. Water (13 mL) and 6,6′-dihydroxy-2,2′-bipyridine (0.185 g, 0.98 mmol) were added, and the mixture was stirred for 1 h at room temperature. After the solution was filtered through a pad of Celite, the solvent was removed in a vacuum to gave a yellow powder of the title product in 84% yield (0.408 g, 0.55 mmol). ^{1}H NMR (400 MHz, D_2O): δ 8.04 (t, J = 8 Hz, 2H, py), 7.83 (d, J = 7 Hz, 2H, py), 7.17 (d, J = 8 Hz, 2H, py), 1.58 (s, 15H, Cp*). ^{13}C NMR (100 MHz, D_2O): δ 164.5 (s, py), 154.1 (s, py), 144.0 (s, py), 120.3 (q, J_{C-F} =317 Hz, OTf), 116.1 (s, py), 114.0 (s, py), 98.1 (d, J_{C-Rh} = 10 Hz, C_5Me_5), 9.2 (s, C_5Me_5).

Preparation of Cp*Rh(bpyO)(H$_2$O) Cat9. Under an atmosphere of argon, $[Cp^*Rh(6,6'\text{-dihydroxy-2,2'-bipyridine})(H_2O)](OTf)_2$ (0.445 g, 0.60 mmol) was placed in a flask. Water (25 mL) and NaO^{t}Bu (0.112 g, 1.2 mmol) were added, and the mixture was stirred for 30 min at room temperature. The yellow solution gradually changed to orange suspension. The suspension was filtered and washed with water (6 mL) and diethylether (5 mL). Drying under vacuum gave **Cat9** as an orange powder (0.238 g, 0.54 mmol, 90%). ^{1}H NMR (400 MHz, CD_3OD): δ 7.44 (t, J = 8 Hz, 2H, py), 6.96 (d, J = 7 Hz, 2H, py), 6.44 (d, J = 9 Hz, 2H, py), 1.58 (s, 15H, Cp*). ^{13}C NMR (100 MHz, CD_3OD): δ 171.7 (s, py), 157.2 (s, py), 140.1 (s, py), 117.9 (s, py), 107.4 (s, py), 96.8 (d, J_{C-Rh} = 9 Hz, C_5Me_5), 9.6 (s, C_5Me_5). Anal. Calcd for $C_{20}H_{23}N_2O_3Rh$: C, 54.31; H, 5.24; N, 6.33. Found: C, 53.77; H, 5.01; N, 6.33.

Preparation of [(HMB)Ru(H$_2$O)$_3$](OTf)$_2$. Under an atmosphere of argon, $[(HMB)RuCl_2]_2$ (0.993 g, 1.5 mmol) was placed in a flask. Water (30 mL) and AgOTf (1.54 g, 6.0 mmol) were added, and the mixture was stirred for 4 h at room temperature. After filtration through a pad of Celite, evaporation of the filtrate gave the title product as an orange powder (1.70 g, 2.9 mmol, 99%). ^{1}H NMR (400 MHz, D_2O): δ 2.19 (s, C_6Me_6). ^{13}C NMR (100 MHz, D_2O): δ 120.3 (q, J_{C-F} = 317 Hz), 89.7 (s, C_6Me_6), 15.8 (s, C_6Me_6).

Preparation of [(HMB)Ru(6,6′-dihydroxy-2,2′-bipyridine)(H$_2$O)](OTf)$_2$. Under an atmosphere of argon, $[(HMB)Ru(H_2O)_3](OTf)_2$ (1.78 g, 3.0 mmol) was placed in a flask. Water (30 mL) and 6,6′-dihydroxy-2,2′-bipyridine (0.594 g, 3.2 mmol) were added, and the mixture was stirred for 2.5 h at room temperature. After the solution was filtered through a pad of Celite, the solvent was removed in a vacuum to give an orange powder of the title product in 77% yield (1.77 g, 2.3 mmol). ^{1}H NMR (500 MHz, D_2O): δ 8.00 (t, J = 8 Hz, 2H, py), 7.81 (d, J = 8 Hz, 2H, py), 7.13 (d, J = 8 Hz, 2H, py), 1.99 (s, 18H, C_6Me_6). ^{13}C NMR (125 MHz, D_2O): δ 166.2 (s, py), 154.6 (s, py), 143.5 (s, py), 120.2 (q, J_{C-F} = 317 Hz), 116.1 (s, py), 113.5 (s, py), 94.7 (s, C_6Me_6), 16.1 (s, C_6Me_6).

Preparation of (HMB)Ru(bpyO)(H$_2$O) (Cat10). Under an atmosphere of argon, $[(HMB)Ru(6,6'\text{-dihydroxy-2,2'-bipyridine})(H_2O)](OTf)_2$ (0.389 g, 0.51 mmol) was placed in a flask. Water (10 mL) and NaO^{t}Bu (0.0983 g, 1.0 mmol) were added, and the mixture was stirred for 1 h at room temperature. The orange solution gradually changed to a green suspension. The suspension was filtered and washed with diethylether (10 mL). Drying under vacuum gave **Cat10** as a green powder (0.192 g, 0.41 mmol, 82%). ^{1}H NMR (400 MHz, CD_3OD): δ 7.41 (t, J = 8 Hz, 2H, py), 6.95 (d, J = 7 Hz, 2H, py), 6.39 (d, J = 8 Hz, 2H, py), 1.99 (s, 18H, C_6Me_6). ^{13}C NMR (100 MHz, CD_3OD): δ 173.6 (s, py), 157.0 (s, py), 139.7 (s, py), 117.2 (s,

py), 107.6 (s, py), 94.4 (s, C_6Me_6), 16.4 (s, C_6Me_6). Anal. Calcd for $C_{22}H_{26}N_2O_3Ru\cdot(H_2O)_3$: C, 50.66; H, 6.18; N, 5.37. Found: C, 50.49; H, 6.06; N, 5.36.

General Procedure for the AAD Reactions Using Cat7, Cat9, and Cat10 Shown in Table 1. Under argon atmosphere, the catalyst (0.50 mol %), benzene (3 mL), and 1-phenylethanol (1.0 mmol) were placed in a flask. The mixture was stirred under vigorous reflux for 20 h. The conversion of 1-phenylethanol and the yield of acetophenone were determined by GC analysis using biphenyl as an internal standard.

■ ASSOCIATED CONTENT

Supporting Information

Optimized geometries of all the species involved in the AAD reaction of 1-phenylethanol **2′** mediated by Cp*Ir(phenO) **1−IrP** and Cp*Rh(bpyO) **1−Rh**, the transition state for the dihydrogen complex formation step in the AAD reaction of ethanol by **1-Ir**, the species in the H_2O dissociation step from **Cat7**, free hydroxypyridine, and the transition state for the direct conversion from **4−Ir** to **5−Ir**. Population changes of Ir, Cp*, C_5N(a), C_5N(b), and O2 along the concerted pathway of the AAD reaction of **2′** by Cp*Ir(bpyO) **1−Ir** and **1−Ru**. The lone pair orbital energies on the O atom of Cp*Ir(bpyO) **1−Ir**, Cp*Ir(phenO) **1−IrP**, and (HMB)Ru(bpyO) **1−Ru**. The Cartesian coordinates of all the species in this work. This material is available free of charge via the Internet at http://pubs.acs.org.

■ AUTHOR INFORMATION

Corresponding Authors

*E-mail: sakaki.shigeyoshi.47e@st.kyoto-u.ac.jp.
*E-mail: fujita.kenichi.6a@kyoto-u.ac.jp.
*E-mail: yamaguchi.ryohei.75s@st.kyoto-u.ac.jp.

Notes

The authors declare no competing financial interest.

■ ACKNOWLEDGMENTS

S.S. acknowledges financial support by the Grants-in-Aid from the Ministry of Education, Culture, Science, Sport, and Technology through Grants-in-Aid of Specially Promoted Science and Technology (no. 22000009). S.S. and G.Z. are also thankful to the computational facility at the Institute of Molecular Science, Okazaki, Japan. K.F. thanks financial support by the Grant-in-Aid for Scientific Research on Innovative Areas (no. 25105732).

■ REFERENCES

(1) (a) Dobereiner, G. E.; Crabtree, R. H. *Chem. Rev.* **2010**, *110*, 681−70. (b) Cheng, C.; Hong, S. H. *Org. Biomol. Chem.* **2011**, *9*, 20−26. (c) Gunanathan, C.; Milstein, D. *Science* **2013**, *341*, 1229712−1−1229712−1.

(2) (a) Friedrich, A.; Schneider, S. *ChemCatChem* **2009**, *1*, 72−73. (b) Johnson, T. C.; Morris, D. J.; Wills, M. *Chem. Soc. Rev.* **2010**, *39*, 81−88. (c) Junge, H.; Loges, B.; Beller, M. *Chem. Commun.* **2007**, 522−524. (d) Nielsen, M.; Kammer, A.; Cozzula, D.; Junge, H.; Gladiali, S.; Beller, M. *Angew. Chem., Int. Ed.* **2011**, *50*, 9593−9597.

(3) (a) Dobson, A.; Robinson, S. D. *J. Organomet. Chem.* **1975**, *87*, C52−C53. (b) Dobson, A.; Robinson, S. D. *Inorg. Chem.* **1977**, *16*, 137−142. (c) Morton, D.; Cole-Hamilton, D. J. *J. Chem. Soc., Chem. Commun.* **1987**, 248−249. (d) Morton, D.; Cole-Hamilton, D. J. *J. Chem. Soc., Chem. Commun.* **1988**, 1154−1156. (e) Ligthart, G. B. W. L.; Meijer, R. H.; Donners, M. P. J.; Meuldijk, J.; Vekemans, J. A. J. M.; Hulshof, L. A. *Tetrahedron Lett.* **2003**, *44*, 1507−1509. (f) Adair, G. R. A.; Williams, J. M. J. *Tetrahedron Lett.* **2005**, *46*, 8233−8235. (g) Robles-Dutenhefner, P. A.; Moura, E. M.; Gama, G. J.; Siebald, H. G. L.; Gusevskaya, E. V. *J. Mol. Catal. A: Chem.* **2000**, *164*, 39−47. (h) Royer, A. M.; Rauchfuss, T. B.; Wilson, S. R. *Inorg. Chem.* **2008**, *47*, 395−397. (i) Baratta, W.; Bossi, G.; Putignano, E.; Rigo, P. *Chem.—Eur. J.* **2011**, *17*, 3474−3481. (j) Prades, A.; Peris, E.; Albrecht, M. *Organometallics* **2011**, *30*, 1162−1167. (k) Musa, S.; Shaposhnikov, I.; Cohen, S.; Gelman, D. *Angew. Chem., Int. Ed.* **2011**, *50*, 3533−3537.

(4) Sieffert, N.; Bühl, M. *J. Am. Chem. Soc.* **2010**, *132*, 8056−8070.

(5) (a) Zhang, J.; Balaraman, E.; Leitus, G.; Milstein, D. *Organometallics* **2011**, *30*, 5716−5724. (b) Zhang, J.; Leitus, G.; Ben-David, Y.; Milstein, D. *J. Am. Chem. Soc.* **2005**, *127*, 10840−10841. (c) Gunanathan, W.; Shimon, L. J. W.; Milstein, D. *J. Am. Chem. Soc.* **2009**, *131*, 3146−3147. (d) Balaraman, E.; Gnanaprakasam, B.; Shimon, L. J. W.; Milstein, D. *J. Am. Chem. Soc.* **2010**, *132*, 16756−16758. (e) Zhang, J.; Gandelman, M.; Shimon, L. J. W.; Rozenberg, H.; Milstein, D. *Organometallics* **2004**, *23*, 4026−4033. (f) Srimani, D.; Balaraman, E.; Gnanaprakasam, B.; Ben-David, Y.; Milstein, D. *Adv. Synth. Catal.* **2012**, *354*, 2403−2406. (g) Gunanathan, C.; Milstein, D. *Acc. Chem. Res.* **2011**, *44*, 588−602.

(6) (a) Zhang, G.; Vasudevan, K. V.; Scott, B. L.; Hanson, S. K. *J. Am. Chem. Soc.* **2013**, *135*, 8668−8681. (b) Zhang, G.; Hanson, S. K. *Org. Lett.* **2013**, *15*, 650−653.

(7) (a) Fujita, K.; Tanino, N.; Yamaguchi, R. *Org. Lett.* **2007**, *9*, 109−111. (b) Yamaguchi, R.; Ikeda, C.; Takahashi, Y.; Fujita, K. *J. Am. Chem. Soc.* **2009**, *131*, 8410−8412. (c) Fujita, K.; Yoshida, T.; Imori, Y.; Yamaguchi, R. *Org. Lett.* **2011**, *13*, 2278−2281. (d) Kawahara, R.; Fujita, K.; Yamaguchi, R. *J. Am. Chem. Soc.* **2012**, *134*, 3643−3646. (e) Kawahara, R.; Fujita, K.; Yamaguchi, R. *Angew. Chem., Int. Ed.* **2012**, *51*, 12790−12794. (f) Nieto, I.; Livings, M. S.; Sacci, J. B. I.; Reuther, L. E.; Zeller, M.; Papish, E. T. *Organometallics* **2011**, *30*, 6339−6342. (g) Hull, J. F.; Himeda, Y.; Wang, W.-H.; Hashiguchi, B.; Periana, R.; Szalda, D. J.; Muckerman, J. T.; Fujita, E. *Nat. Chem.* **2012**, *4*, 383−388. (h) Moore, C. M.; Szymczak, N. K. *Chem. Commun.* **2012**, *49*, 400−402. (i) DePasquale, J.; Nieto, I.; Reuther, L. E.; Herbst-Gervasoni, C. J.; Paul, J. J.; Mochalin, V.; Zeller, M.; Thomas, C. M.; Addison, A. W.; Papish, E. T. *Inorg. Chem.* **2013**, *52*, 9175−9183. (j) Badiei, Y. M.; Wang, W.-H.; Hull, J. F.; Szalda, D. J.; Muckerman, J. T.; Himeda, Y.; Fujita, E. *Inorg. Chem.* **2013**, *52*, 12576−12586.

(8) (a) Zeng, G.; Li, S. *Inorg. Chem.* **2011**, *50*, 10572−10580. (b) Li, H.; Lu, G.; Jiang, J.; Huang, F.; Wang, Z. *Organometallics* **2011**, *30*, 2349−2363. (c) Li, H.; Wang, X.; Huang, F.; Lu, G.; Jiang, J.; Wang, Z. *Organometallics* **2011**, *30*, 5233−5247. (d) Li, H.; Wang, X.; Wen, M.; Wang, Z. *Eur. J. Inorg. Chem.* **2012**, 5011−5020. (e) Li, H.; Wang, Z. *Sci. China: Chem.* **2012**, *55*, 1991−2008. (f) Li, H.; Jiang, J.; Lu, G.; Huang, F.; Wang, Z. *Organometallics* **2011**, *30*, 3131−3141.

(9) The H_2O ligand of the iridium catalyst Cp*Ir(bpyO)(H_2O) **Cat7** is believed to dissociate from the iridium center prior to the AAD reaction. The discussion of the H_2O dissociation step is skipped for brevity in the text, because this process easily occurs and does not directly relate to the AAD reaction; see Figure S2 in SI for energy and geometry changes.

(10) We have attempted the stoichiometric reactions of **Cat7** with benzyl alcohol and 1-phenylethanol in order to isolate **4−Ir**, **5−Ir**, or **7−Ir**. However, isolation of such species was not successful so far.

(11) Lu, G.; Li, H.; Zhao, L.; Huang, F.; Schleyer, P. v. R.; Wang, Z.-X. *Chem.—Eur. J.* **2011**, *17*, 2038−2043.

(12) We have also considered the possibility that water originated from the aquo ligand in **Cat7** serves as a bridging molecule to facilitate the transformation of **4−Ir** into **5−Ir**. The present calculations show that the $\Delta G^{0\neq}$ value is almost the same between the water bridge and the alcohol bridge. If water concentration is enough, both water and alcohol participate in the reaction. This possibility was also examined by the experiment; see also ref 16.

(13) The value of kinetic isotope effect (KIE) in the AAD reaction of 1-phenylethanol catalyzed by **Cat7** was experimentally determined to be 1.27. Such a small KIE value suggests that the rate-determining step would not include the cleavage of the C−H bond, supporting the theoretically predicted mechanism; see also ref 17.

(14) (a) Hashiguchi, S.; Noyori, R. *Acc. Chem. Res.* **1997**, *30*, 97−102. and references therein. (b) Murata, K.; Ikariya, T.; Noyori, R. *J. Org. Chem.* **1999**, *64*, 2186−2187. (c) Mashima, K.; Abe, T.; Tani, K. *Chem. Lett.* **1998**, 1201−1202. (d) Mashima, K.; Abe, T.; Tani, K. *Chem. Lett.* **1998**, 1199−1200. (e) Jiang, Y.; Jiang, Q.; Zhu, G.; Zhang, X. *Tetrahedron Lett.* **1997**, *38*, 215−218. (f) Palmer, M.; Walsgrove, T.; Wills, M. *J. Org. Chem.* **1997**, *62*, 5226−5228. (g) Alonso, D. A.; Guijarro, D.; Pinho, P.; Temme, O.; Andersson, P. G. *J. Org. Chem.* **1998**, *63*, 2749−2751. (h) Jiang, Y.; Jiang, Q.; Zhang, X. *J. Am. Chem. Soc.* **1998**, *120*, 3817−3818.

(15) (a) Carmona, D.; Viguri, F.; Lamata, M. P.; Ferrer, J.; Bardají, E.; Lahoz, F. J.; García-Orduña, P.; Oro, L. A. *Dalton Trans.* **2012**, *41*, 10298−10308. (b) Ogo, S.; Abura, T.; Watanabe, Y. *Organometallics* **2002**, *21*, 2964−2969. (c) Ogo, S.; Kabe, R.; Hayashi, H.; Harada, R.; Fukuzumi, S. *Dalton Trans.* **2006**, 4657−4663. (d) Bennett, M. A.; Mitchell, T. R. B.; Stevens, M. R.; Willis, A. C. *Can. J. Chem.* **2001**, *79*, 655−669. (e) Clapham, S. E.; Hadzovic, A.; Morris, R. H. *Coord. Chem. Rev.* **2004**, *248*, 2201−2237.

(16) When the AAD reaction of 1-phenylethanol catalyzed by **Cat7** (0.5 mol %) was performed in the presence of water (5.0 mol%) under reflux in benzene for 10 min, acetophenone was formed in 70% yield. This result was exactly the same as that of the reaction in the absence of water (yield of acetophenone was 70%). This experimental result is consistent with the computational results (ref 12).

(17) (a) We have also carried out the AAD reaction catalyzed by **Cat7** (0.05 mol%) under reflux in benzene for 20 min using a 1:1 mixture of PhCH(OH)Me and PhCD(OH)Me as starting materials. Conversions of PhCH(OH)Me and PhCD(OH)Me were 38 and 30%, respectively, whereas the yield of acetophenone was 34%. By this result, the value of the kinetic isotope effect was determined to be 1.27. (b) Under the same reaction conditions, (*p*-cymene)Ru(bpyO)(H_2O) exhibits a much lower activity (7% yield) than that (97% yield) by (HMB)Ru(bpyO)(H_2O) **Cat10**.

(18) (a) Hohenberg, P.; Kohn, W. *Phys. Rev.* **1964**, *136*, B864−B871. (b) Kohn, W.; Sham, L. *J. Phys. Rev.* **1965**, *140*, A1133−A1138.

(19) (a) Becke, A. D. *Phys. Rev. A* **1988**, *38*, 3098−3100. (b) Becke, A. D. *J. Chem. Phys.* **1993**, *98*, 5648−5652. (c) Perdew, J. P. In *Electronic Structure of Solids*, 91th ed.; Ziesche, P., Eschrig, H., Eds.; Akademie Verlag: Berlin, 1991. (d) Burke, K.; Perdew, J. P.; Wang, Y. *In Electronic Density Functional Theory: Recent Progress and New Directions*; Dobson, J. F.; Vignale, G.; Das, M. P., Ed.; Plenum: New York, 1998.

(20) (a) Andrae, D.; Haeussermann, U.; Dolg, M.; Stoll, H.; Preuss, H. J. *Theor. Chim. Acta* **1990**, *77*, 123−141. (b) Bergner, A.; Dolg, M.; Kuechle, W.; Stoll, H.; Preuss, H. *Mol. Phys.* **1993**, *80*, 1431−1441.

(21) Dolg, M.; Wedig, U.; Stoll, H.; Preuss, H. *J. Chem. Phys.* **1987**, *86*, 866−872 and see http://www.tc.uni-koeln.de/cgi-bin/pp.pl?language=en,job=getrefs for a complete reference list.

(22) (a) Rassolov, V. A.; Pople, J. A.; Ratner, M. A.; Windus, T. L. *J. Chem. Phys.* **1998**, *109*, 1223−1229. (b) Clark, T.; Chandrasekhar, J.; Spitznagel, G. W.; Schleyer, P. v. R. *J. Comput. Chem.* **1983**, *4*, 294−301. (c) Frisch, M. J.; Pople, J. A.; Binkley, J. S. *J. Chem. Phys.* **1984**, *80*, 3265−3269.

(23) (a) Tomasi, J.; Mennucci, B.; Cammi, R. *Chem. Rev.* **2005**, *105*, 2999−3093. (b) Barone, V.; Cossi, M. *J. Phys. Chem. A* **1998**, *102*, 1995−2001. (c) Cossi, M.; Rega, N.; Scalmani, G.; Barone, V. *J. Comput. Chem.* **2003**, *24*, 669−681.

(24) Mammen, M.; Shakhnovich, E. I.; Deutch, J. M.; Whitesides, G. M. *J. Org. Chem.* **1998**, *63*, 3821−3830.

(25) (a) Ishikawa, A.; Nakao, Y.; Sato, H.; Sakaki, S. *Inorg. Chem.* **2009**, *48*, 8154−8163. (b) Zeng, G.; Sakaki, S. *Inorg. Chem.* **2011**, *50*, 5290−5297. (c) Zeng, G.; Sakaki, S. *Inorg. Chem.* **2012**, *51*, 4597−4605. (d) Aono, S.; Sakaki, S. *J. Phys. Chem. B* **2012**, *116*, 13045−13062.

(26) Frisch, M. J.; Trucks, G. W.; Schlegel, H. B.; Scuseria, G. E.; Robb, M. A.; Cheeseman, J. R.; Scalmani, G.; Barone, V.; Mennucci, B.; Petersson, G. A.; Nakatsuji, H.; Caricato, M.; Li, X.; Hratchian, H. P.; Izmaylov, A. F.; Bloino, J.; Zheng, G.; Sonnenberg, J. L.; Hada, M.; Ehara, M.; Toyota, K.; Fukuda, R.; Hasegawa, J.; Ishida, M.; Nakajima, T.; Honda, Y.; Kitao, O.; Nakai, H.; Vreven, T.; Montgomery, J. A., Jr.; Peralta, J. E.; Ogliaro, F.; Bearpark, M.; Heyd, J. J.; Brothers, E.; Kudin, K. N.; Staroverov, V. N.; Kobayashi, R.; Normand, J.; Raghavachari, K.; Rendell, A.; Burant, J. C.; Iyengar, S. S.; Tomasi, J.; Cossi, M.; Rega, N.; Millam, N. J.; Klene, M.; Knox, J. E.; Cross, J. B.; Bakken, V.; Adamo, C.; Jaramillo, J.; Gomperts, R.; Stratmann, R. E.; Yazyev, O.; Austin, A. J.; Cammi, R.; Pomelli, C.; Ochterski, J. W.; Martin, R. L.; Morokuma, K.; Zakrzewski, V. G.; Voth, G. A.; Salvador, P.; Dannenberg, J. J.; Dapprich, S.; Daniels, A. D.; Farkas, Ö.; Foresman, J. B.; Ortiz, J. V.; Cioslowski, J.; Fox, D. J. *Gaussian 09*, revision B.01; Gaussian, Inc.: Wallingford, CT, 2009.

(27) Grimme, S. *J. Chem. Phys.* **2003**, *118*, 9095−9102.

(28) (a) Trucks, G. W.; Watts, J. D.; Salter, E. A.; Bartlett, R. J. *Chem. Phys. Lett.* **1988**, *153*, 490−495. (b) Trucks, G. W.; Salter, E. A.; Sosa, C.; Bartlett, R. J. *Chem. Phys. Lett.* **1988**, *147*, 359−366.

(29) Civalleri, B.; Zicovich-Wilson, C. M.; Valenzano, L.; Ugliengo, P. *CrystEngComm* **2008**, *10*, 405−410.

(30) Eisen, M. S.; Haskel, A.; Chen, H.; Olmstead, M. M.; Smith, D. P.; Maestre, M. F.; Fish, R. H. *Organometallics* **1995**, *14*, 2806−2812.

(31) Umemoto, T.; Nagayoshi, M.; Adachi, K.; Tomizawa, G. *J. Org. Chem.* **1998**, *63*, 3379−3385.